Earth Planet. Sci. Lett. 678 (2026) 119834

Contents lists available at ScienceDirect

Earth and Planetary Science Letters

journal homepage: www.elsevier.com/locate/epsl

Fluvial responses to climate and tectonics throughout the Quaternary in the semi-arid Andes

A. Binnie [a,*], S.A. Binnie [a], P. Victor [b], J-L. García [c,d], S. Heinze [e], T.J. Dunai [a]

[a] Institute of Geology and Mineralogy, University of Cologne, Zuelpicher Str. 49b, 50674 Cologne, Germany
[b] 4.1 Lithosphere Dynamics, Helmholtz-Zentrum Potsdam Deutsches, GeoForschungsZentrum (GFZ), Telegrafenberg, 14473 Potsdam, Germany
[c] Instituto de Geografía, Pontificia Universidad Católica de Chile, Avenida Vicuña Mackenna 4860, Macul, Santiago 782-0436, Chile
[d] Centro UC Desierto de Atacama, Pontificia Universidad Católica de Chile, Santiago 782-0436, Chile
[e] Institute for Nuclear Physics. University of Cologne, Zuelpicher Str. 77, 50674, Cologne, Germany

ARTICLE INFO

Editor: J.P. Avouac.

Keywords:
Denudation rate
Erosion rate
Cosmogenic nuclides
Huasco River
Central Andes

ABSTRACT

How major shifts in climate over the Quaternary have affected topography is unclear, especially in tectonically active regions. This shortcoming is largely due to a lack of robust chronologies of landscape evolution over the last few million years. Here we document a rare case, where a fluvial landscape has been preserved well enough to record its responses to tectonic and climatic shifts throughout the Quaternary. Our results show that aggradation of sediment fill near the Huasco River mouth in the semi-arid Central Andes at the beginning of the Quaternary corresponds to an increased upstream erosion rate and we propose that this was due to glacial expansion. At 1.3 Ma, the river began to incise into these sediments, and at 1.0 Ma the rate of downcutting increased notably. The fluvial incision coincides with the Early-Middle Pleistocene Transition, when the periodicity of global climate cycles lengthened. We integrate these findings with marine terrace dating in the same region and find that, although fundamental changes of aggradation and incision were coeval with global climate change, the average rates of fluvial incision over million-year timescales are comparable to rates of uplift. Our findings imply that the Central Andean landscape has responded to major shifts in the frequency of orbitally-driven climatic cycles, impacting topography that is governed by tectonic uplift over longer timescales. As the supply of sediments offshore to subduction zones is considered to exert a control on uplift, our results have broader implications for feedbacks between climatic and tectonic processes.

1. Introduction

It has been suggested that episodes of landscape evolution are coeval with major climatic shifts underpinned by Earths orbital parameters (e.g. Bender et al., 2021; Fisher et al., 2023; Godard, et al., 2013). On the other hand, there are several examples where erosion rates have not varied through periods of major global climate change (e.g. Lenard et al., 2020; Oskin et al., 2017) and so the role that climate plays in shaping landscapes, especially those that are tectonically active, remains contentious. Central to this debate is the difficulty of obtaining reliably dated evidence for geomorphologically impactful events over the last several million years, particularly from terrestrial rather than marine settings (Fisher et al., 2023). Given the encompassing nature of global climate shifts, we might expect their influence on the landscape to be readily apparent. However, evolving topography erodes or buries the geomorphic record of its past and it is notoriously difficult to untangle a history of high-magnitude, low-frequency erosional events from secular processes averaged over the long-term (Kirchner et al., 2001). These difficulties are compounded at active plate margins by the need to extricate tectonic influences from any record of landscape change.

One way of addressing this problem is to date the preserved topographic features that may be indicative of changing tectonic and climatic boundary conditions, such as marine and fluvial terraces. Fluvial terrace treads are planed remnants of earlier river levels and may form in alluvial deposits as fill, or fill-cut terraces (Bull, 1991; Merritts et al., 1994). Dating the timing of both sediment aggradation and the fluvial abandonment of terraces cut into those sediments can provide insights into how rivers have responded to tectonic and climatic forcing. Marine terraces, on the other hand, are assumed to form during sea-level highstands (Lajoie, 1986). Relatively consistent Quaternary highstand

* Corresponding author.
E-mail address: ariane.binnie@uni-koeln.de (A. Binnie).

https://doi.org/10.1016/j.epsl.2026.119834
Received 14 June 2025; Received in revised form 27 December 2025; Accepted 8 January 2026
Available online 13 January 2026

elevations (Berends et al., 2021) provide a datum from which the ages and elevations of marine terraces can be used to reconstruct vertical tectonic displacements.

In this study, we derive the timings of fluvial aggradation and incision into those sediments in the semi-arid Andes and combine it with a record of tectonic uplift from marine terrace dating. Valley fill deposits near the Pacific mouth of the Huasco River in central Chile suggest that the fluvial system has adapted to a changing environment and we use cosmogenic nuclide isochron burial dating, surface exposure ages and depth profiles to constrain when the sediments were deposited, the Andean paleoerosion rates that produced them and the timing of subsequent incision. Dating of nearby marine terraces is combined with published, longer-term records to constrain the tectonic uplift history of the area and to compare it with the fluvial incision history of the Huasco River. Coupled with the Quaternary time-span of our ages, this robust chronology of fluvial and marine events allows us to identify the drivers of landscape evolution in relation to both global climatic change and the regional tectonic uplift history.

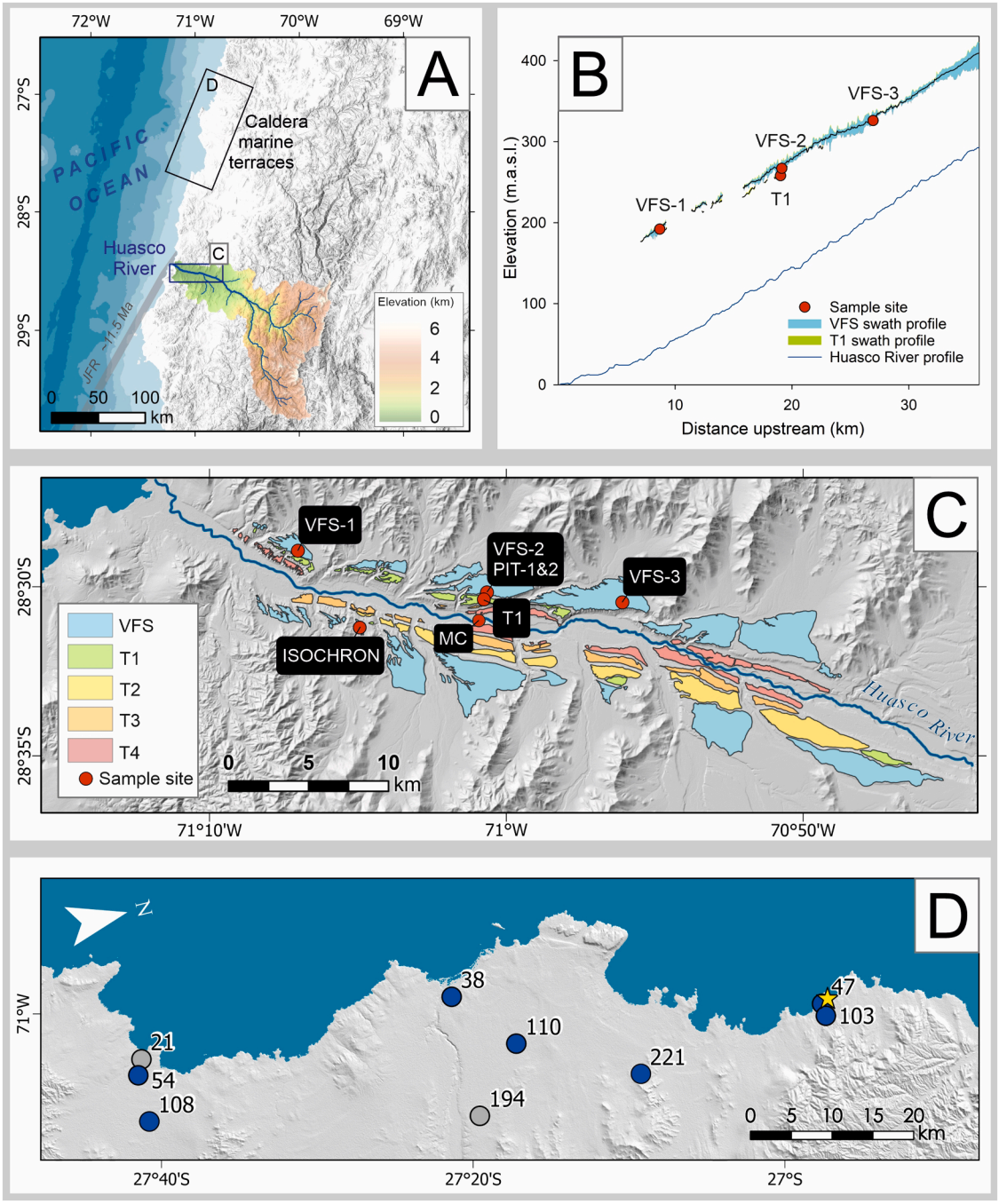

Fig. 1. (A) The Chilean coastline showing the Huasco River catchment and location of the marine terraces sampled at Caldera. The location of the Juan Fernandez Ridge (JFR) around 11.5 Ma is estimated from Le Roux et al. (2005a). (B) Swath profiles showing the elevations of the VFS (valley fill sediment) and T1 (highest fluvial terrace) above the modern bed of the Huasco River. (C) Fluvial terrace surfaces mapped at the mouth of the Huasco Valley, with cosmogenic nuclide dating sampling sites indicated on the valley fill sediment surface (VFS, PIT-1 and PIT-2), within the sediment fill (ISOCHRON), the highest fluvial fill-cut terrace (T1) and the modern sediment from the active channel (MC). (D) The marine terrace sample sites at Caldera are shown by blue circles with the elevations given in meters. The grey circles show sites sampled where age results were indeterminate. The yellow star is the location of the modern beach samples. Background topography and the swath profiles in (B) use ASTER, 1″ (approx. 30 m) resolution digital elevation model data accessed from the NASA Earthdata portal.

2. Background

2.1. Geological setting and uplift history

The Huasco River catchment drains the western flank of the Central Andes Mountains (Fig. 1A). With the headwaters in the Frontal Cordillera, where peaks on the drainage divide exceed elevations of 6 km, the river flows through the more subdued topography of the ~ 1 km high Coastal Cordillera before reaching the Pacific Ocean. Uplift of the Central Andes including the coastal regions is driven by subduction of the Nazca plate beneath the South American plate (Gregory-Wodzicki, 2000). Studies dating the formation age of marine terraces along the coast of central Chile have provided a record of uplift spanning the last several hundred thousand years and uplift rates between 100–400 m/Myr are typical (Regard et al., 2010). Longer-term records of crustal uplift and subsidence come from $^{87}Sr/^{86}Sr$ macro/microfossil dating of coastal sections (LeRoux et al., 2005a, 2005b), which suggests that the southward migration of the subducting Juan Fernández Ridge explains a period of Middle Miocene uplift and subsidence, before the current period of uplift (Fig. 2). This more recent uplift seems to have occurred over the last few Myr, though scatter and some conflicting $^{87}Sr/^{86}Sr$ ages preclude more precise interpretation over Pliocene/Quaternary timescales. Nonetheless, earlier periods of crustal uplift around 12 to 8 Ma followed by subsidence between around 7 to 3 Ma account for the prior deepening of the Huasco Valley, creating the accommodation space for valley fill sediments (VFS) (Fig. 2). The semi-continuous surface of this valley fill can be traced upstream from close to the Pacific mouth of the Huasco River for more than 40 km (Fig. 1C). Close to the coast, the km-wide planar surface of the deposit is perched around 140 m above the modern Huasco River, though the elevation difference between the active channel and the VFS tapers to around 100 m further upstream (Fig. 1B, Fig. 3A). The VFS have thicknesses of 100 - 200 m beneath the current channel (Cabrera et al., 2006; Salas et al., 2016). A similarly planed and elevated fluvial terrace surface, which grades into and is connected to proximal shore platforms, is found close to river mouths further to the south between −30.5°S and 32.5°S (Rodríguez et al., 2013) (Fig. 4A). Interfingering marine layers near to the Huasco river mouth indicate that the fluvial sediments were deposited close to sea-level (Riveros and Riquelme, 2009). Aside from these layers, the general lack of stratification apparent in the matrix supported, fluvially rounded and coarse-grained sediments suggests deposition in an energetic environment (Fig. 3B). The down-cutting of the Huasco River subsequent to the deposition of the valley fill is recorded by a sequence of at least four terraces carved into the sediment (Fig. 1C, Fig. 3A, Fig. S5).

2.2. Climate history

Precipitation along the central and southern Chilean coast is predominantly associated with winter storm tracks of the Southern Hemisphere Westerlies (Garreaud et al., 2009). This source of moisture and the southern limits of Atacama Desert hyperaridity at around 27°S, (Houston., 2006) result in the extreme precipitation gradient along the western side of the Central Andes (Garreaud et al., 2009) (Fig. 4A). Precipitation in the semi-arid zone, where the Huasco catchment lies, is thus sensitive to the northward migration, or intensification, of the Southern Hemisphere Westerlies, as shown by late Quaternary marine (e.g. Hebbeln et al., 2007; Lamy et al., 2001) and terrestrial records (e.g. Garcia et al., 2019; 2024; Heusser, 1990; Veit, 2015).

The high elevations of the semi-arid western Andean flank are currently cold enough to support permanent ice but do not because they lack sufficient rainfall (Ammann et al., 2001; Kull et al., 2002; Sagredo et al., 2014) (Fig. 4B). The migration or intensification of the Westerlies have brought past increases in precipitation to the Andean headwaters of the Huasco catchment, providing the moisture needed for glacial growth (Garcia et al., 2024; Grosjean et al., 1998; Lamy et al., 1998; 2001; Zech et al., 2006). Modeling shows that increased precipitation, along with cooling during the late Pleistocene allowed the glacial

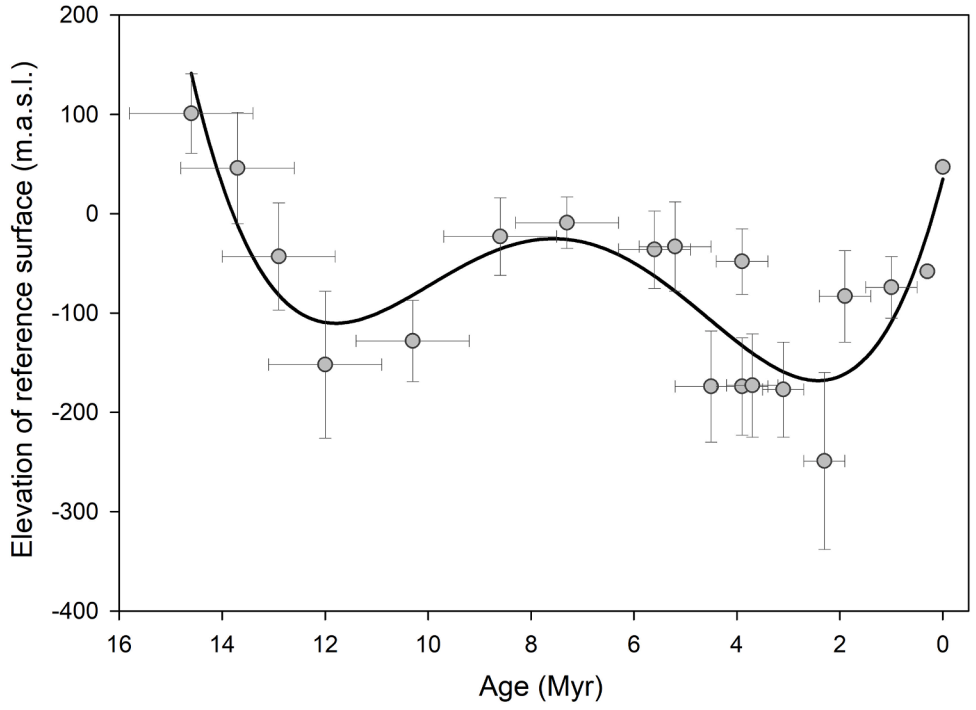

Fig. 2. The uplift and subsidence history of the coast near Huasco since the middle Miocene. Adapted from Le Roux et al. (2005b), who fitted a 4th order polynomial to a chronology of reference surfaces from Carrizalillo (approx. 29°S), dated using fossil assemblages and Sr dating of shells and corrected for variations in sea-level. A similar pattern is observed further south at Tongoy (approximately 30°S) (Le Roux et al., 2005a). The uplift from ~12 Ma to ~8 Ma is interpreted to result from the subduction of the Juan Fernandez Ridge. Uplift, subsidence and then uplift can account for the creation of accommodation space and the subsequent fill of thick (100 - 200 m) sediments beneath the current Huasco River channel (Cabrera et al., 2006; Cabré et al., 2017).

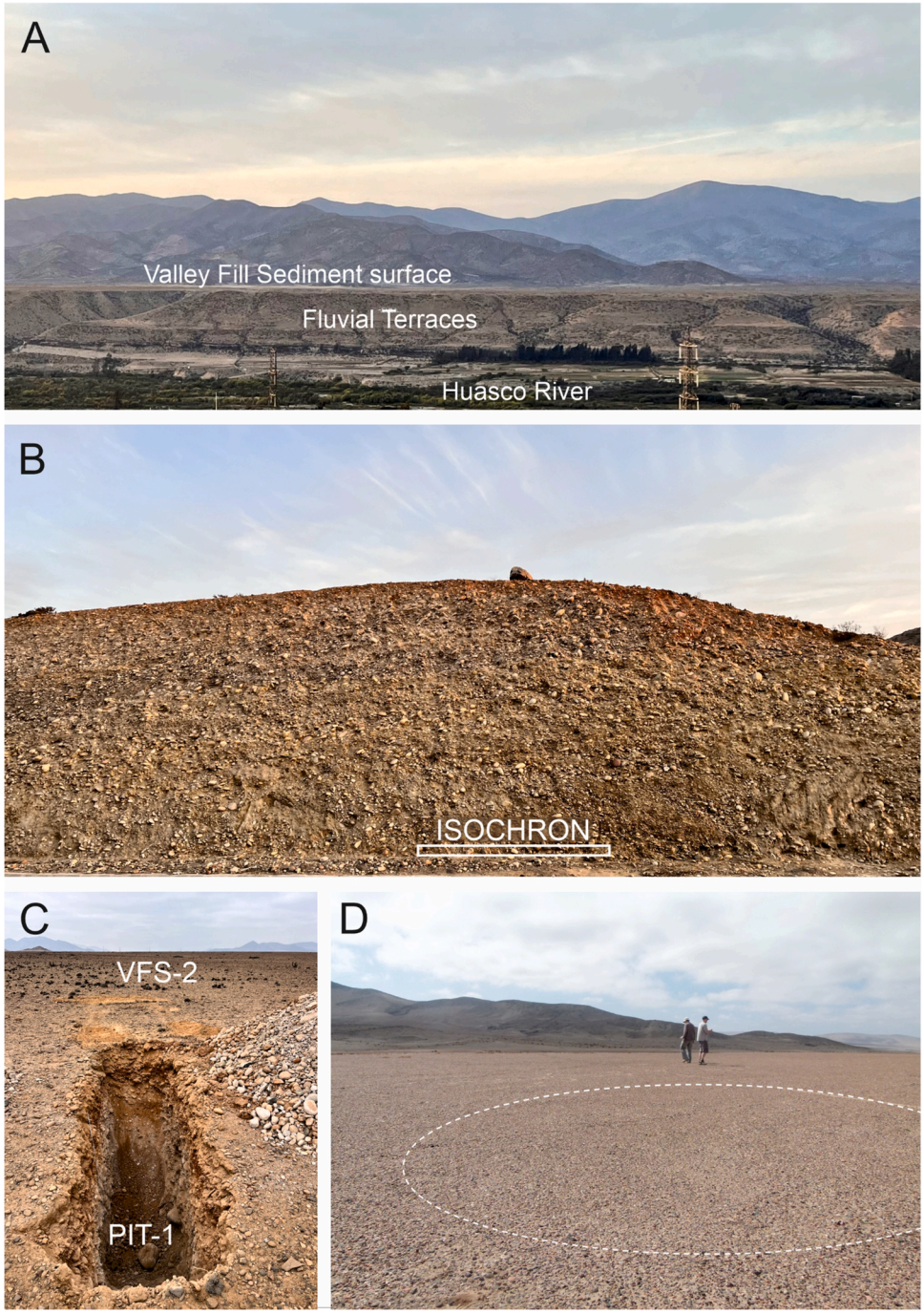

Fig. 3. A. Looking north from the southern bank across the Huasco River at the surface of the Valley Fill Sediment (VFS) and fluvial terraces. B Roadcut through the VFS on the southern side of the Huasco River. The depth of the section shown here is ~ 8 m, showing poorly stratified, fluvially rounded, cobble rich sediments. The opposing side of the roadcut was sampled for isochron burial dating, with the level indicated here (see Fig. 1B). C. PIT-1 depth profile showing the orange/brown upper layers and the cobble rich spoil to the side. In the distance is the surface sampled (VFS-2) for exposure age dating. D. The highest (211 m) marine terrace sample site at Caldera. The planar surface is mantled by a veneer of rounded pebbles. The approximate sample area is indicated by the white dashed line.

equilibrium line altitude (ELA) to descend by over 1000 m to an elevation of 3900 m within the Huasco River catchment (Ammann et al., 2001) (Fig. 4B). The record of this glaciation and of other, less extensive late Pleistocene and Holocene advances are evinced by lateral and terminal moraines (Aguilar et al., 2022; Carraha et al., 2024; Garcia et al., 2024; Zech et al., 2006). These late Pleistocene and Holocene features lie within an even older and more extensively ice-molded Quaternary landscape (Caviedes and Paskoff, 1975).

3. Methods

3.1. Sample collection approach and processing

Cosmogenic nuclides can be used to date the ages of surfaces that are formed as landscapes evolve, as well as the ages of the sediments deposited within those landscapes. To constrain ages of landforms associated with the VFS in the Huasco Valley we used three cosmogenic ^{10}Be and ^{26}Al dating methods, each of which relies on different sampling approaches. All sampling locations discussed below are shown on

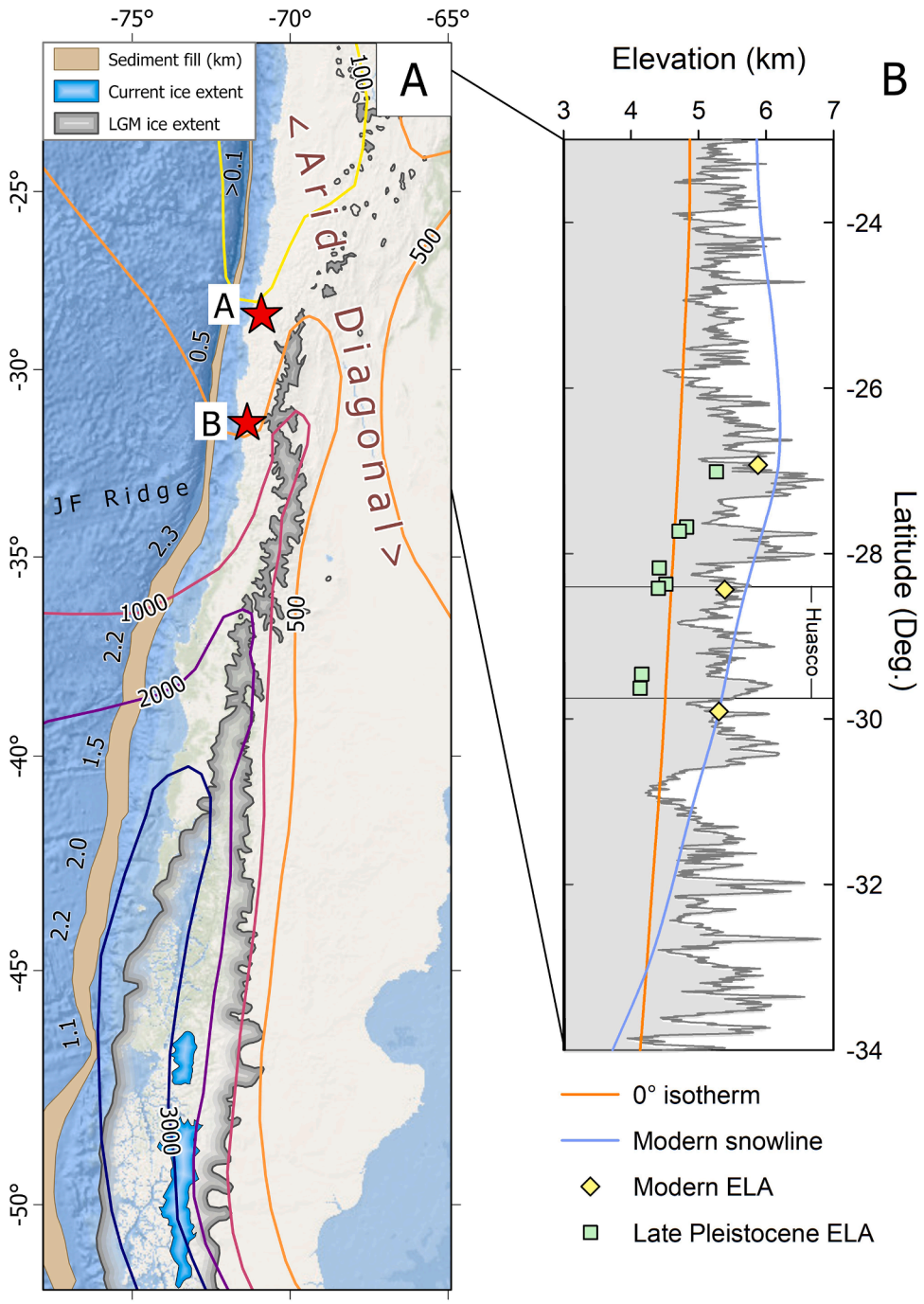

Fig. 4. (A) The limits of the LGM ice in southern South America (Hollin and Schilling, 1981) relative to the location of the dated deposits and surfaces at: A- valley fill of the Huasco River (this study) and B- elevated fluvial surface above the Choapa River (Rodriguiez et al., 2013). The coloured contours give modern mean annual precipitation with the arid diagonal crossing the Andes at around 25–26°S, just to the north of the Huasco River and notable LGM ice extents. The numbers west of the Chilean coast correspond to the km depth of sediments in the trench (Bangs and Cande, 1997) and the current position of the Juan Fernandez Ridge is indicated. (B) The maximum topographic elevations along a latitudinal transition from semi-arid to arid climates are shown by the grey envelope, alongside the zero-degree isotherm and the modern snowline. Elevated portions of the Huasco River catchment lie in a zone of freezing where the current lack of moisture prevents significant glacier growth. The lowering of the ELA during late Pleistocene glacials is, for the most part, attributed to a northward-trending influence of the Southern Westerlies bringing increased precipitation and allowing glacier growth to reach the southern boundary of the Arid Diagonal.

Figs. 1C and 1D We note that for all ^{10}Be and ^{26}Al production rate scaling we apply the LSD scheme of Lifton et al. (2014). We prefer this scheme over others as it accounts for time-dependent magnetic field changes and because it is based on first principle particle flux physics, rather than empirical fits to proxy data sets (see supplementary data).

Firstly, we measured ^{10}Be and ^{26}Al from nine samples and used isochron burial dating to find the depositional age of the sediments of the VFS. For this, cobbles were collected from a roadcut in the VFS on the southern side of the Huasco river from a uniform 10 m depth below the surface (Fig. 3B). Stratification of the exposed section was poor and the coarse, matrix supported sediments were similarly rounded as the sediments in the depth profile pits (see below).

Secondly, we collected six samples from each of two ~1.8 m deep pits (PIT-1 and PIT-2, Fig. 1B and Fig. 3C) dug around 500 m apart into

the VFS to construct ^{10}Be depth profiles, from which we estimated the age of surface formation and inherited concentrations, as well as estimates of surface erosion. Both pits exhibited a grey-brown, less compact, uppermost layer around 20 cm thick. Beneath this was a more reddish-brown horizon, from around 20 to 30 cm, and underlying this until the bottom of the pit was a grey and well cemented layer (Fig. 3C). The coarse fractions of the sediments exposed in the pits were well rounded. Six depths were sampled from each pit. The difficulty in extracting material from the cemented sediments while keeping a narrow depth range meant that all extracted sediment size fractions, from sands to cm-sized pebbles were amalgamated and crushed together. Clasts larger than ~3 cm were avoided when sampling, though individual pebbles might still introduce bias in the concentrations. To consider this, in addition to the amalgamated sediments we measured four single pebbles from the 175 cm depth of PIT-2.

Thirdly, we determined surface exposure ages of individual clasts from the surface of the VFS ($n = 26$) from three separate sites (VFS-1, −2 and −3), and from one site on T1 ($n = 8$), which is the highest fluvial terrace cut into the VFS at around 10 m lower than the surface (Figs. 1B, 1C, 3A). Clear evidence of fluvial rounding, suggesting that minimal erosion of the clast surfaces has occurred since deposition, and no evidence for erosion of the surface that the clasts sat on were primary criteria used for sample selection. The samples from each site were collected from planar surfaces within approximately 10 m of each other. Appreciable distances were kept from the edges of the terrace risers, where buried samples are more likely to be exhumed, and from adjacent hillslopes or risers where there might have been localized colluvial inputs. Site VFS-2 was adjacent to the PIT-1 and −2 locations (Fig. 3C). The other fluvial terraces mapped in the area were not sampled due to concerns over human modification.

Surface exposure age dating was also applied to marine terraces at Caldera (~27°S), from the active shoreline to 221 m elevation (Fig. 1D, Fig. S3 and S4). Sampling and methodological considerations are described in detail by Binnie et al. (2020), who reported the ^{10}Be concentrations of these samples but not the corresponding exposure ages, which we derive here from those results. To summarize the marine terrace sampling, quartz rich clasts were collected from planar portions of five terrace levels (Fig. 3D). Bedrock outcrops on two of these terrace levels were sampled with a hammer and chisel. Pebbles from the modern beach were also sampled.

In addition to dating the terraces and sediment fill, we measured the ^{10}Be concentration of the modern fluvial sediments of the Huasco River (MC on Fig. 1C). The aim of this sampling was to compare the active channel sediment ^{10}Be concentrations and thus upstream erosion rates over relatively recent, millennial, timescales, with the inherited ^{10}Be concentration derived from the depth profiles. The inherited component gives the ^{10}Be concentration of the sediments when they were deposited, meaning it is characteristic of the upstream erosion rates that produced the valley fill sediments.

The samples were prepared as AMS (Accelerator Mass Spectrometry) targets at the University of Cologne using the methods detailed in Binnie et al. (2015). All targets were measured on CologneAMS, with ^{10}Be/^{9}Be and ^{26}Al/^{27}Al normalized to the standards of Nishiizumi et al. (2007) and Nishiizumi et al. (2004), respectively. The ^{10}Be and ^{26}Al concentrations derived from the AMS results were blank corrected by subtracting the atoms in the blank from those in the samples following Binnie et al. (2019). Data tables and sample preparation details are provided in the supplementary information.

3.2. Age, uplift, erosion and incision rate derivations

Burial dating compares the expected surface ratio of a cosmogenic nuclide pair (most often ^{10}Be and ^{26}Al) with the measured ratios from depths sufficient to curtail production, solving for the intervening period of differential decay. The 'horizontal' isochron approach we use here relies on multiple samples from the same depth having variable preburial concentrations, allowing outliers to be identified and minor postburial production to be accounted for. We follow the approach given by Granger et al. (2022), assuming half-lives of ^{10}Be and ^{26}Al of 1.387 ± 0.012 Myr and 708 ± 56 kyr and solving for the burial time and the post-burial ^{10}Be concentration. The ^{26}Al/^{10}Be ratio that samples were buried with is estimated based on the LSD scaling model of Lifton et al. (2014), using an arbitrary preburial exposure time of 100 kyr (e.g. Zhao et al., 2016) and mean elevation and centroid coordinates extracted from a 1 arcsecond ASTER digital elevation model of the Huasco basin. Following Granger et al. (2022), uncertainties in the age and post burial component are derived by Monte Carlo simulation ($n = 10\,000$). As a check of consistency, we calculate postburial ^{10}Be production at our location using LSD and the muogenic scaling provided by Lifton et al. (2014), with surficial, sea level high latitude spallogenic production values taken from Borchers et al. (2016). We assume a density of 2.1 (g/cm^3) is appropriate for the overlying, indurated, cobble rich sediments (Fig. 3) and use a spallogenic attenuation length of 160 g/cm^2.

Cosmogenic nuclide samples taken at different depths can be compared to depth profiles of modelled concentrations to solve for both surface age and erosion, as well as bulk density and the inherited ^{10}Be concentration of the sediments (Anderson et al., 1996). We apply a linear least-squares fit of the equation given in Granger and Smith (2000) for spallogenic and muogenic production with depth, solving for age, erosion, inheritance and density. We use Monte Carlo simulation ($n = 10\,000$) to estimate uncertainties.

Version 3.0 of the online cosmogenic nuclide age calculator of Balco et al. (2008) was used to derive the individual clast surface exposure ages at Huasco and Caldera, applying the default global production rate (Borchers et al., 2016). We assume zero erosion of our clasts due to their preserved fluvially, or wave abraded, rounded form. To approximate the effect of uplift on exposure ages we use an elevation for production rates that is mid-way between the terrace surface and sea-level, or modern river (see supplementary data). The uncertainties of the mean surface exposure ages are the standard deviations of the mean, propagated together with the uncertainty in the global ^{10}Be production rate (7.9 %, Phillips et al., 2016) to give the equivalent of 'external' uncertainties (e.g. Balco et al., 2008). We use version 3.0 of the online calculator of Balco et al. (2008) to approximate the catchment-wide erosion rate and report this with external uncertainties.

Sediments filling the tributary channels that drain into the Huasco River near the coast, plus the sedimentary fill in the broad trunk stream channel, imply it is currently aggrading. Borehole data along the channel bed support this and show the depth of modern sediments is between 40 and 60 m (Cabrera et al., 2006). To account for this in our incision rate estimates we assume an additional 50 ± 10 m elevation difference between the dated surfaces and the Huasco River when it is incising. Incision rates from the VFS, or T1, to the present are then calculated as the quotient of the above derived elevation difference and the average ages of the dated surfaces. The incision rate for the period between the VFS and T1 is the quotient of the elevation difference between VFS-2 and T1 and the age difference of these locations. Uplift rates from the marine terraces are calculated as the elevation difference between sample sites, or to modern sea level, over the age difference between the sites. All uncertainties in the ages and elevations are propagated to estimate the uncertainties of the fluvial incision and uplift rates.

4. Results

For all ^{10}Be and ^{26}Al measurements, blank subtractions amounted to respective reductions of the measured concentrations of < 2 % and individual sample concentrations are given in the supplementary data.

4.1. Timing of VFS aggradation and incision

The results of our isochron dating show that the sediments in the

Huasco Valley were emplaced at 2.59 ± 0.36 Ma (Fig. 5A). Two samples plot below the isochron line, suggesting a previous history of burial prior to emplacement in the VFS and these are not included in the fit. The postburial produced ^{10}Be concentration derived from the intercept of the isochron fit and postburial production line (Fig. 5A) is 5.67 ± 0.62 × 10^4 at/g (1σ), in agreement with the concentration of 6.19 × 10^4 at/g that we calculate over this period of burial based on production at 10 m depth. The MSWD for the isochron fit is 0.34, which might indicate uncertainties are overestimated. Given the thick layers of poorly stratified sediments visible in roadcuts, it seems reasonable to assume that this age represents the timing of deposition to a greater depth than our 10 m deep sampling location. However, marine layers evident in the VFS suggest intervening transgressions and as such the 2.59 Ma age might represent the cessation of a longer period of aggradation.

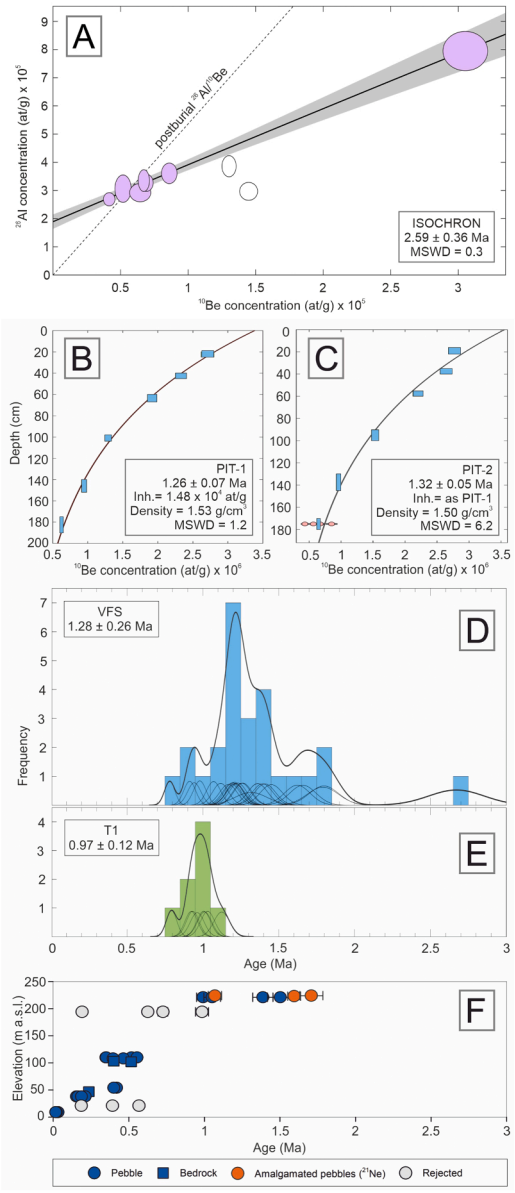

Fig. 5. Ages derived in this study. (A) Isochron of VFS sediments, the grey shaded area around the line is the 1 σ uncertainty. Purple error ellipses are 1 σ and the unfilled ellipses are not included in the fit. The dashed line is the expected postburial ^{26}Al/^{10}Be production ratio at the sampling depth. The ratio (8.29) is derived from the Matlab code of Lifton et al. (2014). (B and C) ^{10}Be concentrations with depth from PIT-1 (B) and PIT-2 (C). Boxes indicate depth range sampled and 1 σ ^{10}Be concentrations. Orange symbols on PIT-2 at 175 cm depth are individual clasts with 1σ uncertainties. Note inheritance (Inh.) at PIT-1 is used to constrain PIT-2. Best fit erosion rates derived for both profiles are close to zero (Fig S6). (D and E) Kernel density estimates overlain on histograms of the exposure ages of the VFS (D) and T1 (E). (F) Age-elevation plot of the marine terraces sampled at Caldera, including recast ages of Quezada et al. (2010). Uncertainties are 1σand levels with no clear age due to scatter shown in grey.

The two depth profiles dug in the surface of the VFS (Figs. 5B and 5C) give ages of 1.26 ± 0.07 Ma and 1.32 ± 0.05 Ma (1σ). The depth profile estimated for PIT-1 shows a good fit with a MSWD of 1.24. Depth profile solutions suggest surface erosion to be negligible, which is substantiated by the lack of topographic relief on the VFS (see also Fig. S6). We obtain a value of 1.53 g/cm^3 for density, although the assumption of uniform density with depth is likely an oversimplification. PIT-2 gives a less well resolved fit, however, given inheritance would not be expected to vary between our sites and because of the robust fit obtained by PIT-1 we constrain inheritance in PIT-2 to be the same as determined for PIT-1, at 1.479 × 10^4 at/g, obtaining an MSWD of 6.2. Using this constraint on inheritance does not significantly impact the quality of the fit, our age and other results, with negligible erosion and a density estimate of 1.50 g/cm^3. The lower density derived from the profiles as compared to that used for the isochron reflects the soil formation and relatively fewer cobbles close to the VFS surface (see Section 3.1). The clasts from 175 cm depth on PIT-2 scatter around a mean value that is in good agreement with the concentration in the amalgamated sample (Fig. 5C) and while the overall fit to PIT-2 is poorer than that of PIT-1 it gives similar results.

The average we obtain for the VFS surface from exposure age dating is 1.28 ± 0.26 Ma (1σ, n = 25) (Fig. 5D). We omit a single sample from this average as it gives a much older age of 2.70 ± 0.38 Ma, though the similarity to the isochron age could point to the survival of this clast at the surface from the time of sediment emplacement. Average ages from the three surface sites of the VFS (VFS-1, −2 and −3) agree within uncertainties, showing this is indeed a single continuous surface (see also Fig. S2). The exposure ages from VFS and T1 display amounts of scatter in excess of their analytical uncertainties, suggesting the potential for surface disturbance. However, ^{26}Al determinations on a subset of the exposure age samples from the VFS sites show no evidence for complex exposure histories (Fig. 6), suggesting they have remained at, or near, the surface throughout their exposure, at least within uncertainties of around 100 kyr. Some scatter in the ^{10}Be concentrations might have originated from samples being brought to the surface shortly after it formed, by deflation or turbation (Binnie et al., 2020). The depth profiles do not suggest notable surface erosion of the VFS but are less sensitive to such processes if they occurred early in the history of the surface. Given that the PIT-2 ^{10}Be concentrations of individual clasts at depth also show a degree of dispersion around the amalgamated sample, variable amounts of pre-exposure seem reasonable to explain excess concentrations and the scatter towards older ages. Because of the good agreement between the average surface exposure age and the ages from the two depth profiles we use an arithmetic mean of the three estimates for the timing of VFS surface abandonment, giving 1.28 ± 0.11 Ma (1 σ). The uncertainty on this age includes the standard deviation of these three measurements (2.9 %) propagated together with the uncertainty in the ^{10}Be production rate (7.9 %, Phillips et al., 2016). The arithmetic mean of the results from T1, the highest fluvial terrace below the surface of the VFS, suggests an age of 973 ± 123 ka (1σ, n = 8) (Fig. 5E).

4.2. Modern versus paleoerosion rates

The ^{10}Be concentration measured in the modern channel sediments is 2.20 ± 0.10 × 10^5 at/g and the basin averaged erosion rate using this concentration is 65 ± 5 m/Myr. The inherited ^{10}Be concentration from PIT-1 is corrected for decay over the 1.28 Myr age of VFS to get a ^{10}Be concentration of 2.80 × 10^4 at/g. The almost order of magnitude lower ^{10}Be concentration suggests upstream erosion was significantly more rapid at the beginning of the Quaternary, when the uppermost VFS were deposited.

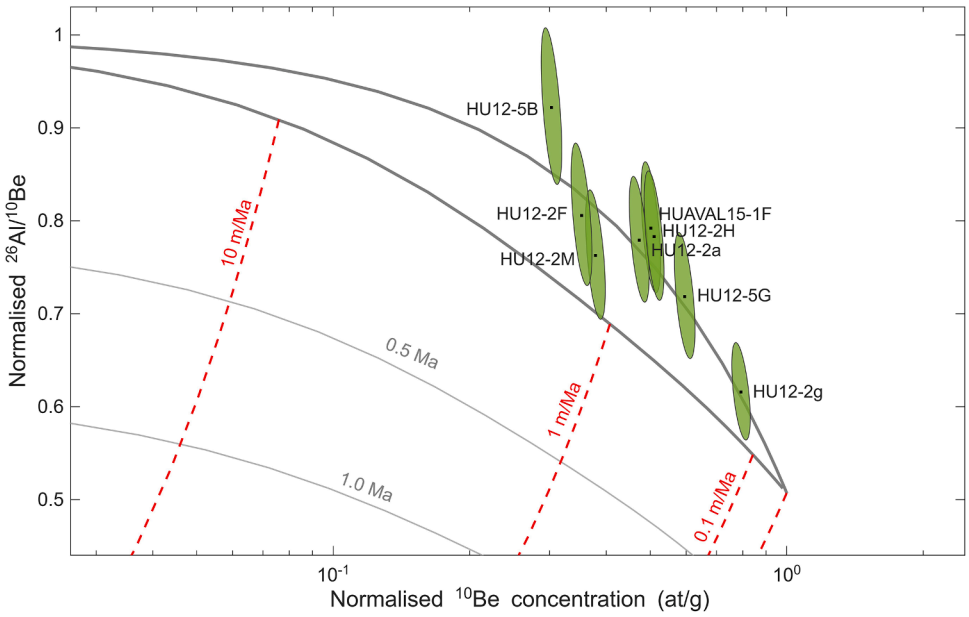

Fig. 6. A two-isotope diagram of ^{10}Be, ^{26}Al pairs to investigate whether samples have undergone appreciable post-exposure burial. Samples are plotted as green ellipses representing two standard deviations. The two dark lines describe constant exposure with no erosion (upper line) and steady-state erosion (lower line), assuming the production rate scaling of Lifton et al. (2014). Samples plotting between these two lines, as seen here, show no indications of lengthy post-depositional burial. Differential decay of ^{26}Al and ^{10}Be mean that samples which have experienced periods of reduced production due to exposure and then cover would plot in the lower region, where red lines denote durations that assume rapid and deep burial.

Our ^{10}Be concentrations in channel sand are comparable to the results of Aguilar et al. (2014), who collected Huasco River sediments ~30 km upstream of our sites. They also found ^{10}Be concentrations are higher in sand than in cobbles. This may mean our results from sands are overestimating the overall channel sediment ^{10}Be concentration, but this effect is not significant enough to account for the difference we find between modern channel sediments ^{10}Be concentrations and those in VFS at the time of deposition.

4.3. Uplift and incision rate histories

The modern shoreline samples at Caldera show ^{10}Be concentrations that are on average 2 % of the oldest terrace concentrations. The highest marine terrace at 211 m suggests a bimodal distribution of ^{10}Be ages, with two pairs of similar ages (Fig. 5F). We use the oldest age from each pair to be compatible with the lower marine terraces, obtaining ages of 1.52 Ma and 1.05 Ma. These results are further supported by previously reported ^{21}Ne data of Quezada et al. (2010) from the same terraces, which we recalculate here to be consistent with our scaling methods (Fig. 5F). Quezada et al. suggested that an inherited ^{21}Ne component explains this age difference, however, given the modern beach samples imply inheritance is only a minor fraction of the total ^{10}Be concentrations at higher elevations, we instead propose that the older pair of ^{10}Be ages represent the most likely formation age for the terrace. The younger ages could result from a later period of reoccupation, whereby the marine terrace was not sufficiently elevated above the surf zone during a subsequent highstand to prevent reworking of terrace deposits (e.g. Malatesta et al., 2022). Or, they represent a period of surface modification, such as an episode of deflation (e.g. Binnie et al., 2020). The slightly older ^{21}Ne ages, as compared to ^{10}Be, might reflect the propensity for stable ^{21}Ne to include prior exposure histories over long timescales. Two of the marine terrace levels (194 m and 21 m) give scattered results that are inconclusive (Fig. 5F). We include them here for completeness but they are excluded from the uplift rate derivations.

The height of the VFS above the modern Huasco River decreases from around 140 m at site VFS-1 to 106 m at site VFS-3. Averaged fluvial incision rates since the abandonment of the VFS to the present day reduce from 148 ± 15 m/Myr closest to the coast, to 122 ± 14 m/Myr 20 km further upstream. The fluvial incision between the locations of VFS-2 and T1 was 32 ± 10 m/Myr from 1.28 Ma until 973 ka, whereupon the average increased to 171 ± 21 m/Myr (Fig. 7). Our marine terrace ages give a relatively constant rate of uplift that averages 211 ± 21 m/Myr between 1.0 Ma to the present and suggests very little uplift occurred between 1.5 Ma and 1.0 Ma ago. Averaging the uplift rates over the 1.5 Ma age of the oldest marine terrace gives 151 ± 14 m/Myr, in good agreement with the rate of fluvial incision into the VFS in proximity to the coast over a similar timescale.

5. Discussion

5.1. Causes and implications of increased Quaternary erosion

At 2.59 ± 0.36 Ma, when the VFS was deposited, erosion rates in the Huasco River catchment were higher. While the increased erosion may appear to be approximately coeval with the shift from subsidence to uplift (Fig. 2) there are three main obstacles to the argument that more rapid erosion, and consequently deposition of the VFS, is linked to this shift. Firstly, the resolution of the ages provided by the ^{87}Sr/^{86}Sr data on which the longer-term, Miocene uplift history is based (LeRoux et al., 2005a) is too coarse to pinpoint tectonic change over the last few million years. The fourth order polynomial that LeRoux et al. fit to this data shows the longer-term trend over the Miocene, but it smooths shorter timescale deviations. Secondly, base-level changes are not communicated upstream rapidly in semi-arid Andean rivers. At locations between 33°S and 35°S, Farias et al. (2008) estimate a long-term knickpoint retreat rate between ~6 – 19 km/Myr, leading them to propose a 5 - 10 Myr lag time between regional uplift and the resulting erosional pulse from knickpoint retreat into the Andean Frontal Cordillera. For our study area, this suggests it would take millions of years after the onset of uplift near the coast before there was an erosional response in the Andes, several tens of kilometers upstream. Thirdly, while the conditions for preservation of the sediments might have been dictated by subsidence and uplift, the erosion and deposition of large amounts of sediment transported from the Andes to the coast, and presumably offshore,

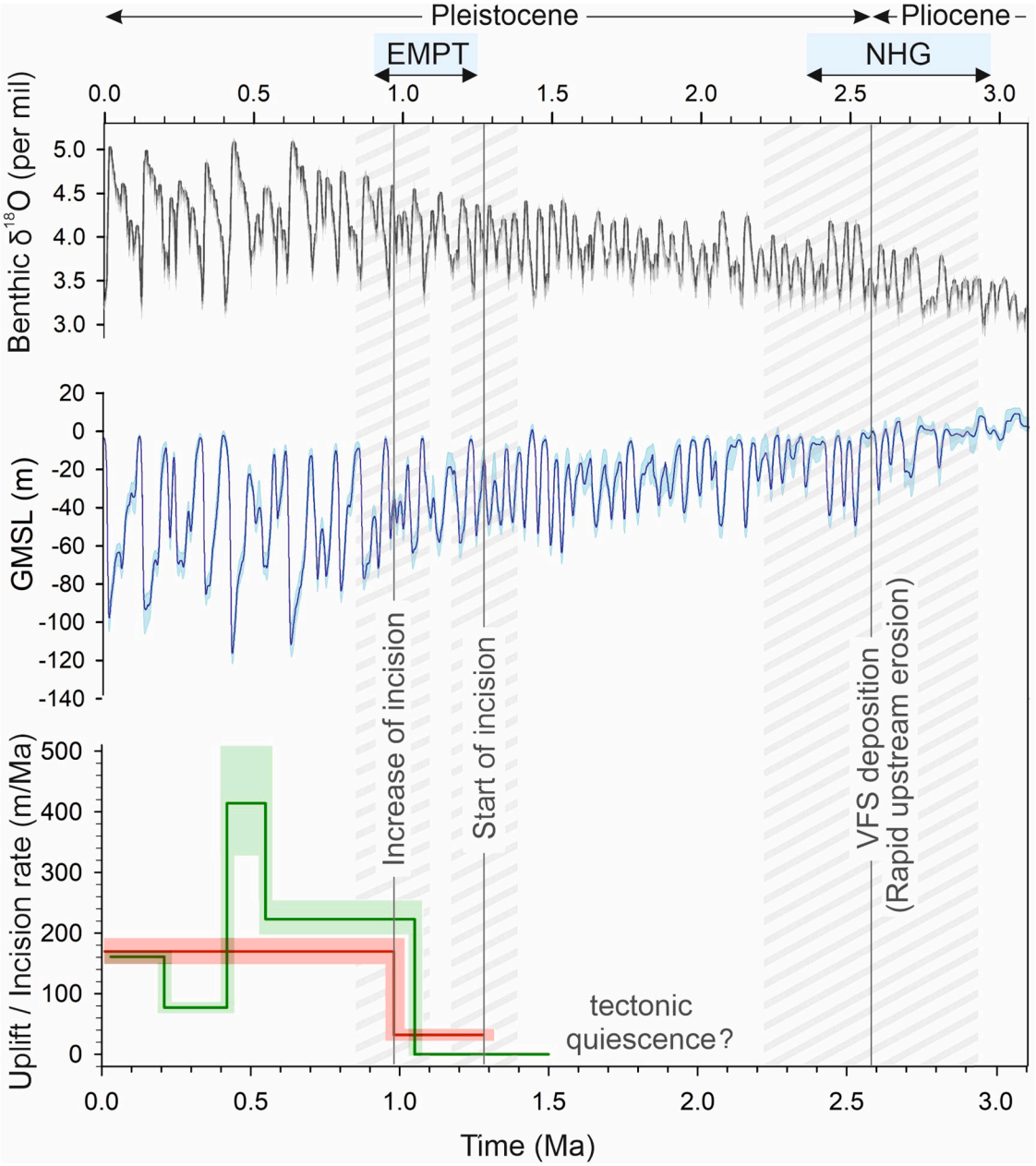

Fig. 7. Late Pliocene/Quaternary variations in climate (Lisiecki and Raymo, 2005) and sea-level (Berends et al., 2021) compared with rates of uplift from marine terrace dating at Caldera (green line) and fluvial incision rates of the Huasco River (red line). NHS is Northern Hemisphere glaciation. VFS aggradation at the onset of the Quaternary corresponds to more rapid upstream erosion. A period of relative stability appears to exist until the onset of the EMPT around 1.3 Ma ago, whereby the Huasco River begins to incise, and at 1 Ma this incision accelerates.

requires increased discharge, as well as a supply of sediments (Bull, 1991). Consequently, a period of subsidence followed by uplift can explain both why the VFS are located near the coast and their preservation over the long-term, but tectonic mechanisms are unlikely to be responsible for the origin of the sediments themselves.

Several studies have argued that increased erosion in the eastern (e.g. Amidon et al., 2017; Fisher et al., 2023; Tofelde et al., 2017) and western (e.g. Carretier et al., 2013) semi-arid Andes can be explained by wetter conditions and increased discharge. Modelling by Fisher et al. (2023) suggests moderate increases of precipitation rate on the order of 20 % are sufficient to drive order of magnitude higher erosion rates in the eastern Central Andes, as compared to the present day. Precipitation in the western Andes is associated with storm tracks of the Southern Westerlies (Garreaud et al., 2009), which have migrated, or intensified northwards and resulted in glaciation in the Central Andes during periods of cooler global climate (see Section 2.2). Incipient glaciations in the Central Andes at the start of the Quaternary would provide a supply of sediments as ice expanded into previously fluvially conditioned, V-shaped topography (Kaplan et al. 2009). Deposits of transport limited, frost-shattered talus produced by periglacial processes, as are presently found in abundance on upper catchment slopes throughout the semi-arid Andes (e.g. Carraha et al., 2024; Caviedes and Paskoff, 1975), would have constituted a further source of readily available sediments. This is analogous, though on a more massive scale, to the ongoing paraglacial response to late Pleistocene glaciation documented in the upper portions of the Huasco River catchment (Cabré et al., 2017). Valley fills are commonly linked to glaciofluvial outwash deposits (Church and Ryder, 1972) and we suggest the correspondence of the rapidly eroded sediments that form the VFS in a catchment whose headwaters would be glaciated under cooler, wetter, conditions implicate a glaciofluvial

origin for the sediments. A basin experiencing glacial erosion would violate some of the assumptions needed to derive accurate paleoerosion rates from cosmogenic nuclide concentrations, and so while the significantly lower concentrations of inherited ^{10}Be in the VFS revealed by the depth profiles show upstream erosion must have been substantially greater when the VFS was deposited, we refrain from giving empirical paleoerosion estimates.

In the eastern Andes, at the same latitude as the Huasco River catchment, a study by Amidon et al. (2017) finds an increase in erosion between 3.3 – 2.9 Myr, peaking at 2.9 Ma. They attribute this to the southern position of the Southern Westerlies during a warm global climate, allowing the South American Low-Level Jet to bring moist air from the Amazon basin into the eastern Central Andes (Garreaud et al., 2009). During a cooler global climate, as the influence of the Southern Westerlies propagates northwards, the eastern Andes become more arid and erosion rates are reduced (Amidon et al., 2017). Thus, the increased erosion that we observe on the western flank, in response to a northward Westerlies influence, is part of an asymmetric pattern of Andean erosion whereby rate increases on the eastern and western flanks are responding to global warming and cooling, respectively. Interestingly, this pattern does not appear in comparisons of eastern and western semi-arid Andean flank erosion rates that average over more recent, mostly Holocene timescales (Val et al., 2018), suggesting asymmetrical erosion occurs only as a response to major climatic change.

5.2. Fluvial responses to climate and tectonics

The general agreement between the highest marine terrace ages at Caldera with the respective ages of the VFS and T1 terrace at Huasco implies a mutual underlying control of terrace formation at both the fluvial and coastal locations. The fluvial and marine terrace ages appear approximately consistent with the initiation and subsequent intensification of the Early-Middle Pleistocene Transition (EMPT) (Fig. 7) (Head and Gibbard., 2015; Mudelsee and Statteger, 1997). This change in the periodicity of global climatic cycles from 41 to 100 kyr began around 1.25 Ma, with the 100 kyr cycles well established by 700 ka (Clark et al., 2006). The time span covered by the transition and the structure within it is still a topic of investigation but the so-called 0.9 Ma 'event' is highlighted in records as corresponding to the first major build-up of northern hemisphere ice (Head and Gibbard, 2015). The character of the EMPT is clear in the benthic δ^{18}O record (Lisiecki and Raymo, 2005) but robustly dated terrestrial examples showing the topographic impact of the transition are rare. There are episodes of Yukon River incision (Bender et al., 2020) at the EMPT, while in the European Alps there is evidence for glacial trough deepening (Hauselmann et al., 2007; Valla et al., 2011). In addition are less well dated but notable examples of major river incision resulting from the longer and more pronounced climate cycles that emerged during the EMPT (Gibbard and Lewin, 2009; Bridgeland and Westaway, 2008), while increased catchment erosion since around 1 Ma has been proposed for the Brazilian highlands (Godard et al., 2024). The EMPT marks marine transgressions and regressions that became less frequent but had greater range, as increased ice-sheet growth consumed an equivalent of 50 m in eustatic sea level (Clark et al., 2006). The longer and more pronounced sea-level fluctuations could form more prominent marine terraces and allow sufficient tectonic uplift to preserve them from the subsequent highstand. More eustatic variability could produce more impactful fluvial base-level changes, with sufficient time between cycles to preserve terraces (Merritts et al., 1994). The rate of fluvial incision of the Huasco River close to the coast is in good agreement with the rate of coastal uplift from the proximal marine terraces at Caldera (Fig. 7). The age offset of few 100 ka between coastal uplift and fluvial incision apparent in Fig. 7 might reflect the time taken to communicate base-level change upstream. Thus, while pivotal climatic changes have left their mark on the Huasco fluvial landscape in the form of eustatically controlled terraces, when averaged over timescales on the order of a million years, a long-term regional uplift rate sets the pace of incision of the Huasco River. This finding agrees with the modeling of Sharma et al. (2021), who propose that erosional responses to global climate cycles are superimposed on longer-term patterns of uplift in settings similar to ours. However, it is also worth noting that the survival of minimally eroded valley fill and terrace surfaces suggests aridity has persisted near the coast for at least the last 1.28 ± 0.11 Ma and so any increased discharge in the Huasco River came from moisture sources upstream of the VFS.

There is an apparent hiatus following the end of sediment aggradation at 2.59 Ma until the VFS surface formation at 1.28 Ma. It is feasible that the 2.59 Ma age does not date the end of deposition and that the formation of the planar VFS at 1.28 Ma was instead the end of a period of lateral channel erosion that has removed interstitial sedimentary evidence, including any landforms pertaining to intervening climate cycles. However, a fluvial process able to plane such a broad, km-wide, low relief surface that extends into tributary valleys, without leaving substantive traces of sediment abandoned at higher elevations along the valley sides seems unlikely. A more feasible explanation is that the sediments were deposited close to sea-level and the surface reworked until 1.28 Ma, whereupon it was abandoned as the Huasco River began to incise. This interpretation is in keeping with the interfingering marine layers near the Huasco River mouth and by the estuarine conditions at 1.0 ± 0.4 Ma that have been recorded at Carrizalillo, ~70 km to the south (Le Roux et al., 2005b).

From 30.5°S to 32.5°S there are near-coast fluvial terraces on several drainages that are similarly elevated above their modern channels as the VFS surface is above the Huasco River, and these are linked to the local highest marine terraces (Rodríguez et al., 2013). The sediments underlying these fluvial terraces correspond to the Confluencia Formation, whose age is poorly constrained to between the Miocene and Pleistocene. The timing of the highest fluvial terrace formation based on a tentative age, which we recast here to be consistent with LSD scaling, is 1.39 ± 0.13 Ma. It thus seems reasonable to extrapolate the chronology we determine for the VFS at Huasco and suggest our ages refer to a more regional event that left its mark close to the coast from 28.5°S to 32.5°S.

5.3. Sediment transport offshore as a linkage between climate and tectonics

The presence of the near-coast VFS that were deposited while upstream erosion rates were significantly higher, as compared with more recent rates, implies that there was a spike in the sediment flux offshore around the onset of the Quaternary, we propose in response to glaciation. Marine core records spanning the LGM from the continental shelf off northern Chile find an input of sediments during glacials, which declines in concert with decreased humidity during deglacials (e.g. Bernhardt et al., 2017; Hebbeln et al., 2007). Variations in the sediment flux offshore to the subduction zone due to Plio-Pleistocene glacial erosion have been associated with Andean subduction dynamics that are particularly relevant for N-S sediment transport processes of trench fill deposits (Bangs and Cande, 1997; Kukowski and Onken, 2006; Melnick and Echtler, 2006). The sediments in the trench are prevented from further northward transport by the bathymetric heights of the Juan Fernandez Ridge, creating a barrier that leads to a much thinner fill north of the ridge (Fig. 4). The persistence of long-term hyperaridity north of the arid-diagonal at ~ 27° make the Huasco River the approximate latitudinal limit of glacially derived sediment from the southern Andes. Between 0.6 to 1 Myr is the estimated time span needed for sediments to be transported from the coast to the trench (Völker et al., 2013) and a further 0.5 Myr for the sediments to be subducted (Bangs and Cande, 1997). Other estimates suggest 2 Myr for the sediments to be entrenched in the subduction zone and to affect behavior of the seismogenic interface (Kukowski and Onken, 2006). An increased sediment supply at the start of the Quaternary would have been entrenched and subducted to seismogenic depths, at the earliest, around

1.5 Ma. Though there are large uncertainties inherent in such estimates, this supply to the trench could have influenced the subduction geodynamics and thus the uplift that we observe after 1.5 Ma.

6. Conclusions

Three key changes in the fluvial history of the Huasco River of Central Chile are the end of aggradation of valley fill following a period of increased upstream erosion, the onset of fluvial downcutting into that massive fill and the subsequent acceleration of the incision rate. These correspond to episodes of major global climatic changes, namely, the cooling associated with the start of the Quaternary, the beginning of the EMPT and the establishment of 100 kyr climate cycles, respectively. Erosion rates were higher at the start of the Quaternary than they have been over the late Pleistocene and we propose this corresponds to the expansion of moisture sensitive glaciers into pre-Quaternary sediment rich high Andean valleys. Compared to other studies, our findings imply an out of phase erosional response between the eastern and western Central Andes, linked to migration of the Southern Westerlies into lower latitudes.

While the timings of major fluvial adjustments appear to have been governed by climate, and in particular by glacio-eustatic sea-level fluctuations, the pace of fluvial incision averaged over the last 1.28 Myr is comparable to rates of uplift over the same timescale. Thus, both shifts in the periodicity of climate cycles and tectonic uplift have been responsible for shaping the active orogenic topography in the Central Andes. The supply of sediment to the subduction zone trench at the start of the Quaternary may be part of a feedback between onshore erosion and subduction processes that include uplift of the coast.

CRediT authorship contribution statement

A. Binnie: Writing – original draft, Methodology, Investigation, Formal analysis. **S.A. Binnie:** Writing – original draft, Supervision, Methodology, Investigation, Funding acquisition, Formal analysis. **P. Victor:** Writing – review & editing, Supervision. **J-L. García:** Writing – review & editing, Investigation. **S. Heinze:** Writing – review & editing, Formal analysis. **T.J. Dunai:** Writing – review & editing, Supervision, Project administration, Methodology, Investigation, Funding acquisition, Conceptualization.

Declaration of competing interest

The authors declare that they have no known competing financial interests or personal relationships that could have appeared to influence the work reported in this paper.

Acknowledgements

The authors acknowledge support from Deutsche Forschungsgemeinschaft (DFG German Research Foundation): grant DU 1028/1-1 (TJD) and Projektnummer 268236062 – SFB 1211 (SAB) and the 'Kids and Elder Care 2020′ program of the University of Cologne (AB). Damian Lopez, Bennedikt Ritter and Elena Voronina are thanked assistance in the laboratory and fieldwork.

Supplementary materials

Supplementary material associated with this article can be found, in the online version, at doi:10.1016/j.epsl.2026.119834.

Data availability

Data available in supplementary information.

References

Aguilar, G., Riquelme, R., Lohse, P., Cabre, A., Garcia, J.L., 2022. Chronology of glacial advances and deglaciation in the Encierro River Valley (29° Lat. S), Southern Atacama Desert, based on geomorphological mapping and cosmogenic be exposure ages. Front. Earth Sci. 10, 878318.
Aguilar, G., et al., 2014. Grain size-dependent Be concentrations in alluvial stream sediment of the Huasco Valley, a semi-arid Andes region. Quat. Geochronol. 19, 163–172.
Amidon, W.H., Fisher, G.B., Burbank, D.W., Ciccioli, P.L., Alonso, R.N., Gorin, A.L., Silverhart, P.H., Kylander-Clark, A.R.C., Christoffersen, M.S., 2017. Mio-Pliocene aridity in the south-central Andes associated with Southern Hemisphere cold periods. Proc. Natl. Acad. Sci. U.S.A. 114 (25), 6474–6479.
Ammann, C., Jenny, B., Kammer, K., Messerli, B., 2001. Late Quaternary Glacier response to humidity changes in the arid Andes of Chile (18-29°S). Palaeogeogr. Palaeoclimatol. Palaeoecol. 172 (3–4), 313–326.
Anderson, R.S., Repka, J.L., Dick, G.S., 1996. Explicit treatment of inheritance in dating depositional surfaces using in situ (super 10) Be and (super 26) Al. Geology 24 (1), 47–51.
Balco, G., Stone, J.O., Lifton, N.A., Dunai, T.J., 2008. A complete and easily accessible means of calculating surface exposure ages or erosion rates from 10Be and 26Al measurements. Quat. Geochronol. 3 (3), 174–195.
Bangs, N.L., Cande, S.C., 1997. Episodic development of a convergent margin inferred from structures and processes along the southern Chile margin. Tectonics 16 (3), 489–503.
Bender, A.M., Lease, R.O., Corbett, L.B., Bierman, P.R., Caffee, M.W., Rittenour, T.M., 2020. Late Cenozoic climate change paces landscape adjustments to Yukon River capture. Nat. Geosci. 13 (8), 571–575.
Berends, C.J., de Boer, B., van de Wal, R.S.W., 2021. Reconstructing the evolution of ice sheets, sea level, and atmospheric CO2 during the past 3.6 million years. Clim. Past 17 (1), 361–377.
Bernhardt, A., Schwanghart, W., Hebbeln, D., Stuut, J.-B.W., Strecker, M.R., 2017. Immediate propagation of deglacial environmental change to deep-marine turbidite systems along the Chile convergent margin. Earth Planet. Sci. Lett. 473, 190–204.
Binnie, A., Binnie, S.A., Parteli, E.J.R., Dunai, T.J., 2020. The implications of sampling approach and geomorphological processes for cosmogenic Be-10 exposure dating of marine terraces. Nucl. Instrum. Methods Phys. Res. B-Beam Interact. Mater. At. 467, 130–139.
Binnie, S.A., Dunai, T.J., Voronina, E., Goral, T., Heinze, S., Dewald, A., 2015. Separation of Be and Al for AMS using single-step column chromatography. Nucl. Instrum. Methods Phys. Res. B: Beam Interact. Mater. At. 361, 397–401.
Binnie, S.A., Dewald, A., Heinze, S., Voronina, E., Hein, A., Wittmann, H., von Blanckenburg, F., Hetzel, R., Christl, M., Schaller, M., Leanni, L., Hippe, K., Vockenhuber, C., Ivy-Ochs, S., Maden, C., Fulop, R.H., Fink, D., Wilcken, K.M., Fujioka, T., Fabel, D., Freeman, S.P.H.T., Xu, S., Fifield, L.K., Akcar, N., Spiegel, C., Dunai, T.J., Aumaitre, G., Bourles, D.L., Keddadouche, K., Team, A., 2019. Preliminary results of CoQtz-N: a quartz reference material for terrestrial in situ cosmogenic Be-10 and Al-26 measurements. Nucl. Instrum. Methods Phys. Res. B-Beam Interact. Mater. At. 456, 203–212.
Borchers, B., Marrero, S., Balco, G., Caffee, M., Goehring, B., Lifton, N., Nishiizumi, K., Phillips, F., Schaefer, J., Stone, J., 2016. Geological calibration of spallation production rates in the CRONUS-Earth project. Quat. Geochronol. 31, 188–198.
Bridgland, D., Westaway, R., 2008. Climatically controlled river terrace staircases: a worldwide Quaternary phenomenon. Geomorphology 98 (3–4), 285–315.
Bull, W.B., 1991. Geomorphic Responses to Climatic Change. Oxford Univ. Press, New York, NY, p. 326.
Cabré, C.A., Aguilar, M.G., Riquelme, S.R., 2017. Holocene evolution and geochronology of a semiarid fluvial system in the western slope of the Central Andes: AMS 14 C data in El Tránsito River Valley, Northern Chile. Quat. Int. 438, 20–32.
Cabrera, G., et al., 2006. Estudio De Calidad de Aguas Subterraneas En Les Cuencas de Huasco y Maquito: Gobierno de Chile - Comision Nacional de Riego Secretaria Ejecutiva. Departamento Technico.
Carraha, J., García, J.L., Nussbaumer, S.U., Fernández-Navarro, H., Gärtner-Roer, I., 2024. Late Pleistocene to Holocene glacial, periglacial, and paraglacial geomorphology of the upper Río Limarí basin (30-31° S) in the Andes of central Chile. J. Maps 20 (1).
Carretier, S., Regard, V., Vassallo, R., Aguilar, G., Martinod, J., Riquelme, R., Pepin, E., Charrier, R., Hérail, G., Farías, M., Guyot, J.L., Vargas, G., Lagane, C., 2013. Slope and climate variability control of erosion in the Andes of central Chile. Geology 41 (2), 195–198.
Caviedes, C., Paskoff, R., 1975. Quaternary Glaciations in the Andes of North-Central Chile. J. Glaciol. 14, 155–170.
Church, M., Ryder, J.M., 1972. Paraglacial Sedimentation - a Consideration of Fluvial Processes Conditioned by Glaciation. Geol. Soc. Am. Bull. 83 (10), 3059.
Clark, P.U., Archer, D., Pollard, D., Blum, J.D., Rial, J.A., Brovkin, V., Mix, A.C., Pisias, N. G., Roy, M., 2006. The middle Pleistocene transition:: characteristics. mechanisms, and implications for long-term changes in atmospheric PCO. Quat. Sci. Rev. 25 (23–24), 3150–3184.
Farías, M., Charrier, R., Carretier, S., Martinod, J., Fock, A., Campbell, D., Cáceres, J., Comte, D., 2008. Late Miocene high and rapid surface uplift and its erosional response in the Andes of central Chile (33°-35°S). Tectonics 27 (1).
Fisher, G.B., Luna, L.V., Amidon, W.H., Burbank, D.W., De Boer, B., Stap, L.B., Bookhagen, B., Godard, V., Oskin, M.E., Alonso, R.N., Tuenter, E., Lourens, L.J., 2023. Milankovitch-paced erosion in the southern Central Andes. Nat. Commun. 14 (1).

García, J.L., Carraha, J., Fernández-Navarro, H., Nussbaumer, S.U., Pérez, F., Hidy, A.J., Gärtner-Roer, I., Haeberli, W., 2024. Glacial to periglacial transition at the end of the last ice age in the subtropical semiarid Andes. Geomorphology 465.
García, J.L., Andrade, B., Calderón, M., Lüthgens, C., 2019. Multi-millennial scale climate variability during MIS 3 and MIS 2 inferred from luminescence dating of coastal sand dunes and buried paleosol sequences in central Chile, 32°S. J. Quat. Sci. 34 (3), 203–214.
Garreaud, R.D., Vuille, M., Compagnucci, R., Marengo, J., 2009. Present-day South American climate. Palaeogeogr. Palaeoclimatol. Palaeoecol. 281 (3–4), 180–195.
Gibbard, P.L., Lewin, J., 2009. River incision and terrace formation in the Late Cenozoic of Europe. Tectonophysics 474 (1–2), 41–55.
Godard, V., Siame, L.L., Salgado, A.A.R., team, A.S.T.E.R., 2024. Erosional Response to Pleistocene Climate Changes in the Brazilian Highlands. J. Geophys. Res.: Earth Surf. 129.
Godard, V., Tucker, G.E., Fisher, G.B., Burbank, D.W., Bookhagen, B., 2013. Frequency-dependent landscape response to climatic forcing. Geophys. Res. Lett. 40 (5), 859–863.
Granger, D.E., Smith, A.L., 2000. Dating buried sediments using radioactive decay and muogenic production of 26Al and 10Be. Nucl. Instrum. Methods Phys. Res. B 172 (1–4), 822–826.
Granger, D.E., Stratford, D., Bruxelles, L., Gibbon, R.J., Clarke, R.J., Kuman, K., 2022. Cosmogenic nuclide dating of Australopithecus at Sterkfontein, South Africa. Proc. Natl. Acad. Sci. U.S.A. 119, 27.
Gregory-Wodzicki, K.M., 2000. Uplift history of the Central and Northern Andes: a review. Geol. Soc. Am. Bull. 112 (7), 1091–1105.
Grosjean, M., Geyh, M.A., Messerli, B., Schreier, H., Veit, H., 1998. A late-Holocene (< 2600 BP) glacial advance in the south-central Andes (29 degrees S), northern Chile. Holocene 8 (4), 473–479.
Haeuselmann, P., Granger, D.E., Jeannin, P.Y., Lauritzen, S.E., 2007. Abrupt glacial valley incision at 0.8 Ma dated from cave deposits in Switzerland. Geology 35 (2), 143–146.
Head, M.J., Gibbard, P.L., 2015. Early–Middle Pleistocene transitions: linking terrestrial and marine realms. Quat. Int. 389, 7–46.
Hebbeln, D., Lamy, F., Mohtadi, M., Echtler, H., 2007. Tracing the impact of glacial-interglacial climate variability on erosion of the southern Andes. Geology 35 (2).
Heusser, C.J., 1990. Ice-Age Vegetation and Climate of Subtropical Chile. Palaeogeogr. Palaeoclimatol. Palaeoecol. 80 (2), 107–127.
Hollin, J.T., Schilling, D.H., 1981. Late Wisconsin-Weichselian Mountain Glaciers and Small Ice Caps. In: Denton, G.H., Hughes, T.J. (Eds.), The Last Great Ice Sheets. Wiley, New York, pp. 179–206.
Houston, J., 2006. Variability of precipitation in the Atacama Desert: its causes and hydrological impact. Int. J. Climatol. 26 (15), 2181–2198.
Kaplan, M.R., Hein, A.S., Hubbard, A., Lax, S.M., 2009. Can glacial erosion limit the extent of glaciation? Geomorphology 103 (2), 172–179.
Kirchner, J.W., Finkel, R.C., Riebe, C.S., Granger, D.E., Clayton, J.L., King, J.G., Megahan, W.F., 2001. Mountain erosion over 10 yr, 10 k.y., and 10 my. Time Scales: Geol. 29 (7), 591–594.
Kukowski, N., Oncken, O., 2006. Subduction Erosion - the "Normal" Mode of Fore-Arc Material Transfer along the Chilean Margin?: andes. Act. Subduction Orogeny 217–236.
Kull, C., Grosjean, M., Veit, H., 2002. Modeling modern and Late Pleistocene glacio-climatological conditions in the north Chilean Andes (29-30 degrees S). Clim. Change 52 (3), 359–381.
Lajoie, K.R., 1986. Coastal tectonics. In: Wallace, R.E. (Ed.), Active Tectonics. National Academics Press, Washington DC, pp. 95–124.
Lamy, F., Hebbeln, D., Wefer, G., 1998. Late quaternary precessional cycles of terrigenous sediment input off the Norte Chico, Chile (27.5 degrees S) and palaeoclimatic implications. Palaeogeogr. Palaeoclimatol. Palaeoecol. 141 (3–4), 233–251.
Lamy, F., Hebbeln, D., Rohl, U., Wefer, G., 2001. Holocene rainfall variability in southern Chile: a marine record of latitudinal shifts of the Southern Westerlies. Earth Planet. Sci. Lett 185 (3–4), 369–382.
Lenard, S.J.P., Lave, J.M., France-Lanord, C., Aumaitre, G., Bourles, D.L., Keddadouche, K., 2020. Steady erosion rates in the Himalayas through late Cenozoic climatic changes. Nat. Geosci. 13 (6), 448–452.
Le Roux, J.P., Gomez, C.A., Olivares, D.M., Middleton, H., 2005a. Determining the Neogene behavior of the Nazca plate by geohistory analysis. Geology 33 (3), 165–168.
Le Roux, J.P., Gómez, C., Venegas, C., Fenner, J., Middleton, H., Marchant, M., Buchbinder, B., Frassinetti, D., Marquardt, C., Gregory-Wodzicki, K.M., Lavenu, A., 2005b. Neogene-Quaternary coastal and offshore sedimentation in north central Chile: record of sea-level changes and implications for Andean tectonism. J. South Am. Earth Sci. 19, 83–98.
Lifton, N., Sato, T., Dunai, T.J., 2014. Scaling in situ cosmogenic nuclide production rates using analytical approximations to atmospheric cosmic-ray fluxes. Earth Planet. Sci. Lett. 386, 149–160.
Lisiecki, L.E., Raymo, M.E., 2005. A Pliocene-Pleistocene stack of 57 globally distributed benthic delta O-18 records (vol 20, art no PA1003, 2005). Paleoceanography 20 (2).
Malatesta, L.C., Finnegan, N.J., Huppert, K.L., Carreño, E., 2022. The influence of rock uplift rate on the formation and preservation of individual marine terraces during multiple sea-level stands. Geology 50 (1), 101–105.
Melnick, D., Echtler, H.P., 2006. Inversion of forearc basins in south-central Chile caused by rapid glacial age trench fill. Geology 34 (9), 709–712.
Merritts, D.J., Vincent, K.R., Wohl, E.E., 1994. Long river profiles, tectonism, and eustasy: a guide to interpreting fluvial terraces. J. Geophys. Res.: Solid Earth 99 (B7), 14031–14050.
Mudelsee, M., Stattegger, K., 1997. Exploring the structure of the mid-Pleistocene revolution with advanced methods of time series analysis. Geol. Rundsch. 86 (2), 499–511.
Nishiizumi, K., Imamura, M., Caffee, M.W., Southon, J.R., Finkel, R.C., McAninch, J., 2007. Absolute calibration of Be-10 AMS standards. Nucl. Instrum. Methods Phys. Res. B-Beam Interact. Mater. At. 258 (2), 403–413.
Nishiizumi, K., 2004. Preparation of Al-26 AMS standards. Nucl. Instrum. Methods Phys. Res. B-Beam Interact. Mater. At. 223, 388–392.
Oskin, M.E., Longinotti, N.E., Peryam, T.C., Dorsey, R.J., DeBoer, C.J., Housen, B.A., Blisniuk, K.D., 2017. Steady Be-derived paleoerosion rates across the Plio-Pleistocene climate transition, Fish Creek-Vallecito basin, California. J. Geophys. Res.-Earth Surf. 122 (9), 1653–1677.
Phillips, F.M., Argento, D.C., Balco, G., Caffee, M.W., Clem, J., Dunai, T.J., Finkel, R., Goehring, B., Gosse, J.C., Hudson, A.M., Jull, A.J.T., Kelly, M.A., Kurz, M., Lal, D., Lifton, N., Marrero, S.M., Nishiizumi, K., Reedy, R.C., Schaefer, J., Stone, J.O.H., Swanson, T., Zreda, M.G., 2016. The CRONUS-Earth Project: a synthesis. Quat. Geochronol. 31, 119–154.
Quezada, J., Gonzalez, G., Dunai, T., Jensen, A., Juez-Larre, J., 2010. Pleistocene littoral uplift of northern Chile: 21Ne age of the upper marine terrace of Caldera-Bahía Inglesa area. Rev. Geol. Chile 34, 81–96.
Regard, V., Saillard, M., Martinod, J., Audin, L., Carretier, S., Pedoja, K., Riquelme, R., Paredes, P., Hérail, G., 2010. Renewed uplift of the Central Andes Forearc revealed by coastal evolution during the Quaternary. Earth Planet. Sci. Lett. 297 (1–2), 199–210.
Riveros, K., Riquelme, R., 2009. In: Morfoestratigrafía neógena-cuaternaria de la cuenca delrío Huasco, norte de Chile: Implicancias eustáticas, tectónicas y climáticas en eldesarrollo de un sistema fluvial en el antearco externo de los Andes centrales, 22. XII Congreso Geológico Chileno, Santiago.
Rodríguez, M.P., Carretier, S., Charrier, R., Saillard, M., Regard, V., Hérail, G., Hall, S., Farber, D., Audin, L., 2013. Geochronology of pediments and marine terraces in north-central Chile and their implications for Quaternary uplift in the Western Andes. Geomorphology 180-181, 33–46.
Sagredo, E.A., Rupper, S., Lowell, T.V., 2014. Sensitivities of the equilibrium line altitude to temperature and precipitation changes along the Andes. Quat. Res. 81 (2), 355–366.
Salas, I., Herrera, C., Luque, J.A., Delgado, J., Urrutia, J., Jordan, T., 2016. Recent climatic events controlling the hydrological and the aquifer dynamics at arid areas: the case of Huasco River watershed, northern Chile. Sci. Total Environ. 571, 178–194.
Sharma, H., Ehlers, T.A., Glotzbach, C., Schmid, M., Tielbörger, K., 2021. Effect of rock uplift and Milankovitch timescale variations in precipitation and vegetation cover on catchment erosion rates. Earth Surf. Dyn. 9 (4), 1045–1072.
Tofelde, S., Schildgen, T.F., Savi, S., Pingel, H., Wickert, A.D., Bookhagen, B., Wittmann, H., Alonso, R.N., Cottle, J., Strecker, M.R., 2017. 100 kyr fluvial cut-and-fill terrace cycles since the Middle Pleistocene in the southern Central Andes, NW Argentina. Earth Planet. Sci. Lett. 473, 141–153.
Val, P., Venerdini, A.L., Ouimet, W., Alvarado, P., Hoke, G.D., 2018. Tectonic control of erosion in the southern Central Andes. Earth Planet. Sci. Lett. 482, 160–170.
Valla, P.G., Shuster, D.L., van der Beek, P.A., 2011. Significant increase in relief of the European Alps during mid-Pleistocene glaciations. Nat. Geosci. 4 (10), 688–692.
Veit, H., Preusser, F., Trauerstein, M., 2015. The Southern Westerlies in Central Chile during the two last glacial cycles as documented by coastal aeolian sand deposits and intercalating palaeosols. Catena 134, 30–40.
Völker, D., Geersen, J., Contreras-Reyes, E., Reichert, C., 2013. Sedimentary fill of the Chile Trench (32-46°S): volumetric distribution and causal factors. J. Geol. Soc. Lond. 170 (5), 723–736.
Zech, R., Kull, C., Veit, H., 2006. Late Quaternary glacial history in the Encierro Valley, northern Chile (29 degrees S), deduced from Be-10 surface exposure dating. Palaeogeogr. Palaeoclimatol. Palaeoecol. 234 (2–4), 277–286.
Zhao, Z.J., Granger, D., Zhang, M.H., Kong, X.G., Yang, S.L., Chen, Y., Hu, E.Y., 2016. A test of the isochron burial dating method on fluvial gravels within the Pulu volcanic sequence, West Kunlun Mountains, China. Quat. Geochronol. 34, 75–80.